

Phonon transport of Janus monolayer MoSSe: a first-principles study

San-Dong Guo

School of Physics, China University of Mining and Technology, Xuzhou 221116, Jiangsu, China

Transition Metal Dichalcogenide (TMD) monolayers have most widely studied due to their unique physical properties. Recently, Janus TMD Monolayer MoSSe with sandwiched S-Mo-Se structure has been synthesized by replacing the top S atomic layer in MoS₂ with Se atoms. In this work, we systematically investigate the phonon transport and lattice thermal conductivity (κ_L) of MoSSe monolayer by first-principles calculations and linearized phonon Boltzmann equation within the single-mode relaxation time approximation (RTA). Calculated results show that the κ_L of MoSSe monolayer is very lower than that of MoS₂ monolayer, and higher than that of MoSe₂ monolayer. The corresponding sheet thermal conductance of MoSSe monolayer is 342.50 WK⁻¹ at room temperature. These can be understood by phonon group velocities and lifetimes. Compared with MoS₂ monolayer, the smaller group velocities and shorter phonon lifetimes of MoSSe monolayer give rise to lower κ_L . The larger group velocities for MoSSe than MoSe₂ monolayer is main reason of higher κ_L . The elastic properties of MoS₂, MoSSe and MoSe₂ monolayers are also calculated, and the order of Young's modulus is identical with that of κ_L . Calculated results show that isotope scattering leads to 5.8% reduce of κ_L . The size effects on the κ_L are also considered, which is usually used in the device implementation. When the characteristic length of MoSSe monolayer is about 110 nm, the κ_L reduces to half. These results may offer perspectives on thermal management of MoSSe monolayer for applications of thermoelectrics, thermal circuits and nanoelectronics, and motivate further theoretical or experimental efforts to investigate thermal transports of Janus TMD monolayers.

PACS numbers: 72.15.Jf, 71.20.-b, 71.70.Ej, 79.10.-n

Email:sandongyuwang@163.com

Keywords: Lattice thermal conductivity; Group velocities; Phonon lifetimes

I. INTRODUCTION

Due to many novel properties, two-dimensional (2D) materials have been attracting increasing attention since the discovery of graphene¹. The TMD², group-VA^{3,4}, group IV-VI⁵ and group-IV⁶ monolayers have been predicted theoretically or synthesized experimentally, which have potential applications in electronic, thermoelectric, quantum and optoelectronic devices. Recently, Janus monolayer MoSSe has been synthesized, based on MoS₂ monolayer by breaking the out-of-plane structural symmetry⁷. The existence of vertical dipoles has been proved by second harmonic generation and piezoresponse force microscopy measurements⁷. The strong piezoelectric effects have been predicted in monolayer and multilayer Janus TMD MXY (M = Mo and W; X/Y = S, Se and Te) by first-principles calculations⁸, which has potential applications in energy harvesting and sensors. Electronic and optical properties have been studied in pristine Janus MoSSe and WSSe monolayers and their vertical and lateral heterostructures⁹. The ZrSSe monolayer has also been predicted with the 1T phase¹⁰, which is different from MoSSe monolayer with 2H phase. It is proved that ZrSSe monolayer has better n-type thermoelectric properties than monolayer ZrS₂.

The thermal property of 2D materials is quite worth studying due to its importance on the performance and reliability on the nano-devices. As is well known, a high thermal conductivity can effectively remove the accumulated heat, while a low thermal conductivity is beneficial to thermoelectric applications. In theory, thermal transports of many 2D materials have

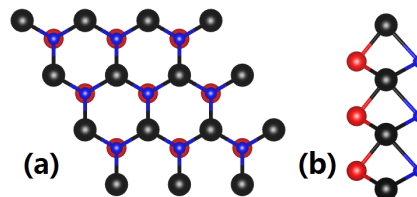


FIG. 1. (Color online) Top (Right) and side (Left) views of crystal structure of MoSSe monolayer. The large black balls represent Mo atoms, and the middle red balls for Se atoms, and the small blue balls for S atoms.

been widely studied¹¹⁻²⁷, such as TMD, group-VA, ATeI (A=Sb or Bi), group IV-VI and group-IV monolayers. It is found that strain can effectively tune κ_L for various kinds of 2D materials, such as group-IV monolayers^{23,26,27}, MoTe₂¹⁹, antimonene²⁵ and Penta-Structures monolayers²⁴. With strain increasing, the κ_L shows monotonous increase/decrease and up-and-down behavior, and tensile strain can induce strong size effects on κ_L . The phonon transports of TMD MX₂ (M=Mo, W, Zr and Hf; X=S and Se) monolayers have been systematically studied by phonon Boltzmann transport equation approach¹¹. The κ_L of 2H-type TMD monolayers are generally higher than those of 1T-type ones, which can be attributed to the large acoustic-optical frequency gap¹¹. In this work, the phonon transport of Janus TMD MoSSe monolayer is performed from a combination of first-principles calculations and linearized phonon Boltzmann equation. It is found that the κ_L of MoSSe monolayer is very lower than that of MoS₂ monolayer, but higher than one of MoSe₂ monolayer. The order of their

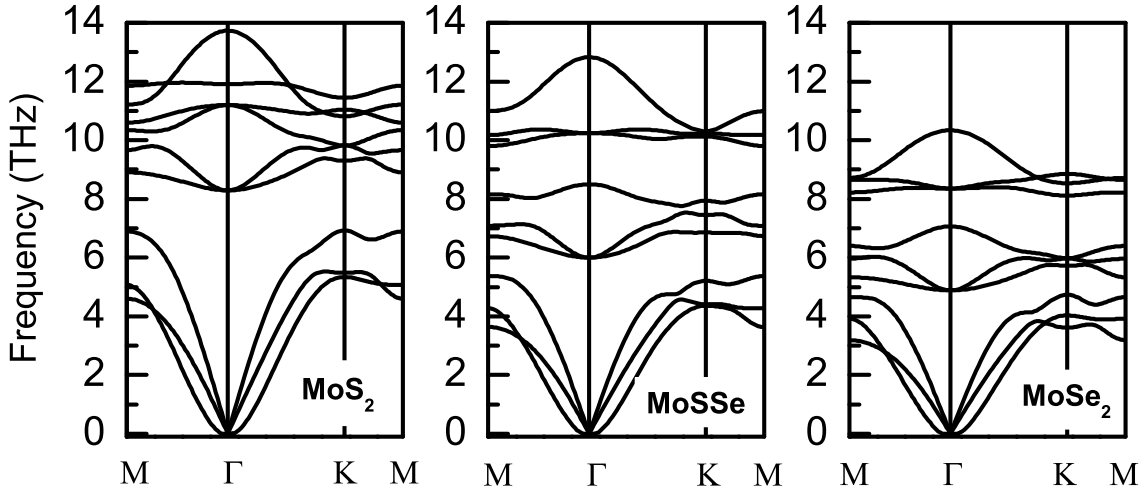


FIG. 2. Phonon dispersion curves of MoS₂, MoSSe and MoSe₂ monolayers.

TABLE I. Lattice constants a and related bond lengths of MoS₂, MoSSe and MoSe₂ monolayers in Å.

Name	a	d_{Mo-S}	d_{Mo-Se}	$d_{S/Se-S/Se}$
MoS ₂	3.18 (3.17 ⁷)	2.41	-	3.12
MoSSe	3.25 (3.23 ⁷)	2.42	2.54	3.23
MoSe ₂	3.30 (3.30 ⁷)	-	2.54	3.35

κ_L is explored by phonon group velocities and lifetimes. It is found that the order of Young's modulus (MoS₂ > MoSSe > MoSe₂) is identical with that of κ_L , which accords with the relation: $\kappa_L \sim \sqrt{E}$ ²⁸. The isotope and size effects on κ_L are also studied, which can provide valuable information for designing MoSSe-based nano-electronics devices.

The rest of the paper is organized as follows. In the next section, the computational details about phonon transport calculations are given. In the third section, the phonon transport and elastic properties of MoSSe monolayer, together with ones of MoS₂ and MoSe₂ monolayers for a comparison, are shown. Finally, we shall give some discussions and conclusions in the fourth section.

II. COMPUTATIONAL DETAIL

Within projector augmented-wave method, we perform the first-principles calculations using the VASP code²⁹⁻³² by adopting generalized gradient approximation of Perdew-Burke-Ernzerhof (PBE-GGA) as exchange-correlation functional³². During structural relaxation, a $20 \times 20 \times 1$ k-mesh is used with a Hellman-Feynman force convergence threshold of 10^{-4} eV/Å. A plane-wave basis set is employed with kinetic energy cutoff of 450 eV, and the electronic stopping criterion is 10^{-8} eV. The 5s and 4d electrons of Mo, and 3/4s and 3/4p electrons of S/Se are treated as valance

ones. The lattice thermal conductivity is performed by using Phono3py+VASP codes^{29-31,33}. By solving linearized phonon Boltzmann equation, the κ_L is calculated with single-mode RTA, as implemented in the Phono3py code³³. The κ_L can be expressed as:

$$\kappa = \frac{1}{NV_0} \sum_{\lambda} \kappa_{\lambda} = \frac{1}{NV_0} \sum_{\lambda} C_{\lambda} \nu_{\lambda} \otimes \nu_{\lambda} \tau_{\lambda} \quad (1)$$

in which λ , N and V_0 are phonon mode, the total number of q points sampling Brillouin zone (BZ) and the volume of a unit cell, and C_{λ} , ν_{λ} , τ_{λ} is the specific heat, phonon velocity, phonon lifetime. The phonon lifetime τ_{λ} can be attained by phonon linewidth $2\Gamma_{\lambda}(\omega_{\lambda})$ of the phonon mode λ :

$$\tau_{\lambda} = \frac{1}{2\Gamma_{\lambda}(\omega_{\lambda})} \quad (2)$$

The $\Gamma_{\lambda}(\omega)$ takes the form analogous to the Fermi golden rule:

$$\Gamma_{\lambda}(\omega) = \frac{18\pi}{\hbar^2} \sum_{\lambda'\lambda''} |\Phi_{-\lambda\lambda'\lambda''}|^2 [(f'_{\lambda} + f''_{\lambda} + 1)\delta(\omega - \omega'_{\lambda} - \omega''_{\lambda}) + (f'_{\lambda} - f''_{\lambda})[\delta(\omega + \omega'_{\lambda} - \omega''_{\lambda}) - \delta(\omega - \omega'_{\lambda} + \omega''_{\lambda})]] \quad (3)$$

in which f_{λ} and $\Phi_{-\lambda\lambda'\lambda''}$ are the phonon equilibrium occupancy and the strength of interaction among the three phonons λ , λ' , and λ'' involved in the scattering. Based on the supercell approach with finite atomic displacement of 0.03 Å, the second-order interatomic force constants (IFCs) can be attained by using a $5 \times 5 \times 1$ supercell with k-point meshes of $2 \times 2 \times 1$. According to second-order harmonic IFCs, phonon dispersions can be calculated by Phonopy package³⁴. The third-order IFCs can be attained by using a $3 \times 3 \times 1$ supercell with k-point meshes of $3 \times 3 \times 1$. To compute accurately lattice thermal conductivity, the reciprocal spaces of the primitive cells are sampled by $100 \times 100 \times 1$ meshes.

TABLE II. The calculated optical phonon frequencies (THz) of MoS₂, MoSSe and MoSe₂ monolayers at the Γ point with experimental results given in parentheses.

Name	E''	E'	A' ₁	A'' ₂
MoS ₂	8.29 (8.49 ³⁶)	11.20 (11.55 ³⁶)	11.91 (12.12 ³⁶)	13.73 (14.10 ³⁶)
MoSSe	6.00	10.24 (10.65 ⁷)	8.50 (8.64 ⁷)	12.83
MoSe ₂	4.88 (5.01 ³⁷)	8.35(8.46 ³⁷)	7.06 (7.20 ³⁷)	10.34 (10.53 ³⁷)

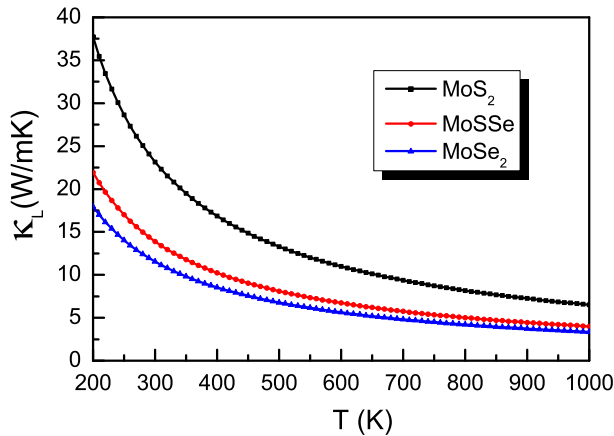


FIG. 3. (Color online) The lattice thermal conductivities of MoS₂, MoSSe and MoSe₂ monolayers as a function of temperature.

For 2D material, the calculated lattice thermal conductivity depends on the length of unit cell along z direction³⁵. They should be normalized by multiplying Lz/d , where Lz and d are the length of unit cell along z direction and the thickness of 2D material. However, the d is not well defined, for example graphene. In this work, the $Lz=24.64$ Å is used as d . By $\kappa \times d$, the thermal sheet conductance can be attained.

III. MAIN CALCULATED RESULTS AND ANALYSIS

The structure of Janus MoSSe monolayer is similar to MoS₂/MoSe₂ monolayer with the 2H phase, containing three atomic sublayers with Mo layer sandwiched between S and Se layers. The Janus monolayer MoSSe can be constructed by replacing one of two S (Se) layers with Se (S) atoms in MoS₂ (MoSe₂) monolayer. The schematic crystal structure of MoSSe monolayer is plotted in Figure 1. It is clearly seen that the Janus MoSSe monolayer loses the reflection symmetry with respect to the central metal Mo atoms compared with MoS₂/MoSe₂ monolayer. Therefore, the MoSSe monolayer (No.156) has lower symmetry compared with MoS₂/MoSe₂ monolayer (No.187). To avoid spurious interaction between neighboring layers, the unit cell of Janus MoSSe monolayer, containing one Mo, one S and one Se atoms, is constructed with the vacuum region of more than 18 Å. The optimized lattice

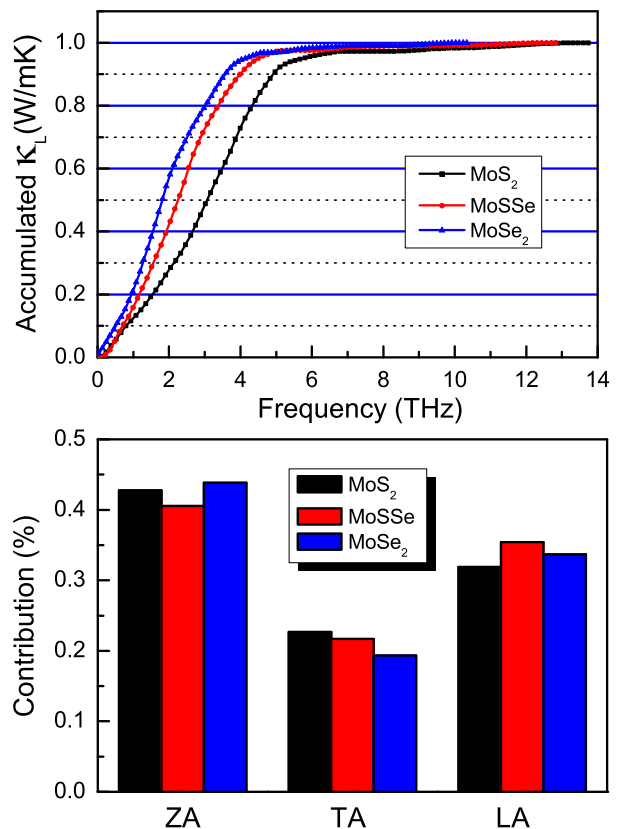


FIG. 4. (Color online) For MoS₂, MoSSe and MoSe₂ monolayers: Top: the ratio between accumulated and total lattice thermal conductivity with respect to frequency. Bottom: the phonon modes contributions toward total lattice thermal conductivity from ZA, TA and LA acoustic phonon branches.

constants (other theoretical values⁷) and bond lengths of MoS₂, MoSSe and MoSe₂ monolayers are listed in Table I. It is expected that a of MoSSe monolayer is between ones of MoS₂ and MoSe₂ monolayers, which is about 2.2% higher than that of MoS₂ monolayer, and 1.5% lower than that of MoSe₂ monolayer. It is noted that the bond length of Mo-S/Se between MoSSe and MoS₂/Se₂ monolayers is almost the same. The bond length of S-Se of MoSSe monolayer is between ones of S-S (MoS₂) and Se-Se (MoSe₂).

Figure 2 shows the phonon dispersions of MoS₂, MoSSe and MoSe₂ monolayers along high symmetry path, which agree well with previous results^{7,11,16}. The 3 acoustic and 6 optical phonon branches are observed due to three

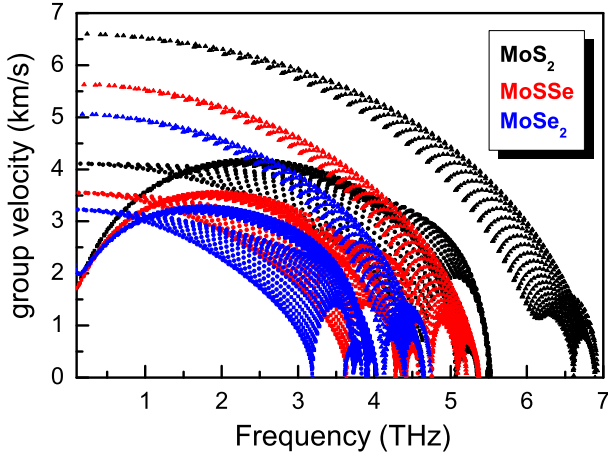


FIG. 5. (Color online) The phonon mode group velocities of MoS₂ (Black), MoSSe (Red) and MoSe₂ (Blue) monolayers in the first BZ for ZA (square symbol), TA (circle symbol) and LA (UpTriangle symbol) acoustic branches.

atoms in the unit cell. The longitudinal acoustic (LA) and transversal acoustic (TA) branches are linear near the Γ point, while out-of-plane acoustic (ZA) branch deviates from linearity. Similar behavior can be found in many 2D materials^{12–16,20–27}. Due to D_{3h} symmetry for MoS₂, MoSSe and MoSe₂ monolayers, the optical lattice-vibration modes at Γ point can be defined as:

$$\Gamma_{optical} \equiv A_2''(IR) + A_1'(R) + E'(IR + R) + E''(R) \quad (4)$$

in which IR and R mean infrared- and Raman-active mode, respectively. The optical phonon frequencies of MoS₂, MoSSe and MoSe₂ monolayers at the Γ point along with available experimental values are listed in Table II. The calculated phonon frequencies of MoS₂ and MoSe₂ monolayers are in agreement with the experimental results^{7,36,37}. From MoS₂ to MoSSe to MoSe₂ monolayer, acoustic modes become softened, and the optical branches overall move toward lower energy, which mean reduced group velocities. A frequency gap between the acoustic and optical phonon branches can be observed, which is due to mass differences between the constituent atoms^{38,39}. The frequency gap is 1.36 THz for MoS₂, 0.63 THz for MoSSe and 0.15 THz for MoSe₂. The frequency gap along with the width of acoustic branches are listed in Table III, which agree well with available theoretical results^{11,16}. It is noted that the frequency gap can produce important influence on acoustic+acoustic→optical (aao) scattering¹¹. The large gap induces ineffective aao scattering due to the requirement on energy conservation, while small gap results in much more frequent aao scattering. These have important effects on phonon transports of both bulk and 2D materials^{11,40,41}.

Within RTA method, Figure 3 shows the intrinsic lattice thermal conductivities of MoS₂, MoSSe and MoSe₂ monolayers from harmonic and anharmonic IFCs. With the same thickness d (24.64 Å), the room-temperature

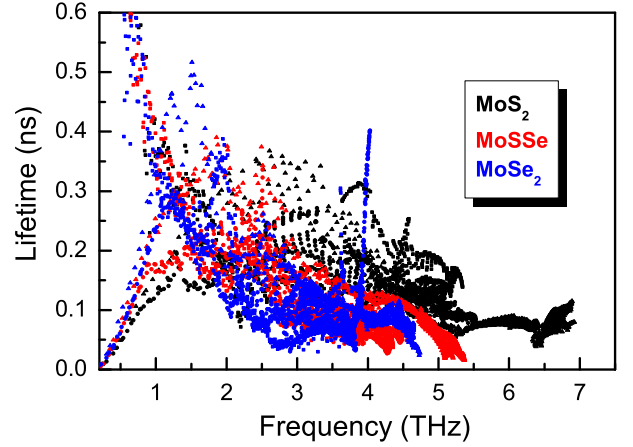


FIG. 6. (Color online) The phonon mode lifetimes of MoS₂ (Black), MoSSe (Red) and MoSe₂ (Blue) monolayers in the first BZ for ZA (square symbol), TA (circle symbol) and LA (UpTriangle symbol) acoustic branches.

TABLE III. The frequency gap between the acoustic and optical phonon branches G_{ao} (THz); the width of acoustic branches W_a (THz); thermal sheet conductance κ_L (WK⁻¹).

Name	G_{ao}	W_a	κ_L
MoS ₂	1.36 (1.35 ¹¹)	6.93 (6.90 ¹¹ , 7.01 ¹⁶)	570.42 (509.84 ¹¹)
MoSSe	0.63	5.37	342.50
MoSe ₂	0.15	4.74 (4.73 ¹⁶)	284.35 (307.33 ¹¹)

lattice thermal conductivity is 23.15 Wm⁻¹K⁻¹, 13.90 Wm⁻¹K⁻¹ and 11.54 Wm⁻¹K⁻¹, respectively. Their thermal sheet conductance³⁵ is 570.42 WK⁻¹, 342.50 WK⁻¹ and 284.35 WK⁻¹, respectively. The thermal sheet conductances of MoS₂, MoSSe and MoSe₂ monolayers are listed in Table III, together with reported theoretical values¹¹ using similar RTA method, which have been converted into thermal sheet conductances. Our calculated values of MoS₂ and MoSe₂ monolayers are very close to previous ones¹¹. It is expected that the lattice thermal conductivity of MoSSe monolayer is between ones of MoS₂ and MoSe₂ monolayers. In the considered temperature range, the κ_L of MoSSe monolayer is about 60% of one of MoS₂ monolayer, and around 121% of κ_L of MoSe₂. For MoS₂, MoSSe and MoSe₂ monolayers, the ratio between accumulated and total lattice thermal conductivity with respect to frequency are plotted in Figure 4 at room temperature. It is clearly seen that acoustic branches of MoS₂, MoSSe and MoSe₂ monolayers dominate lattice thermal conductivity, providing a contribution of 97.3%, 97.6% and 96.9%, respectively. The relative contribution of every phonon mode of acoustic branches to the total lattice thermal conductivity (300 K) also are shown in Figure 4. It is found that the order of contribution is ZA > LA > TA for all three monolayers, and about 42% for ZA mode, 33% for TA mode and 21% for LA mode.

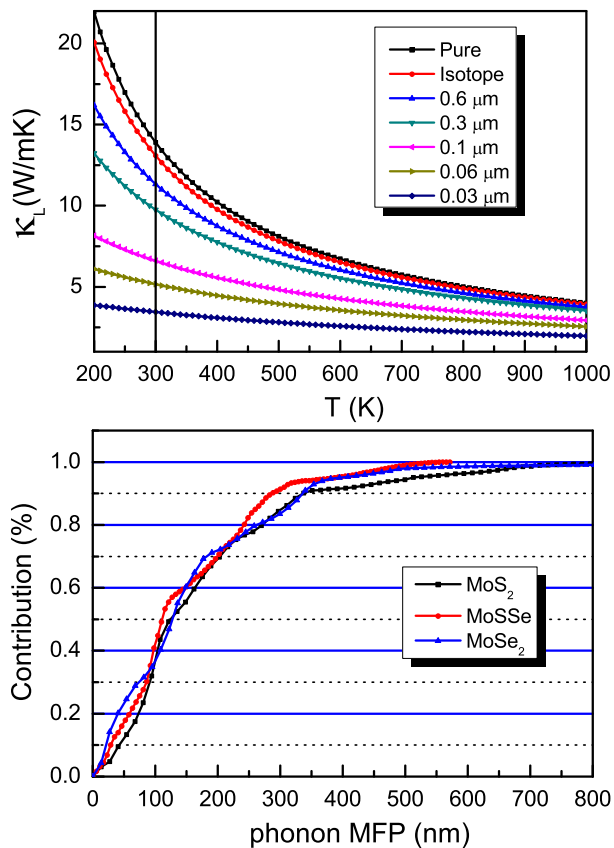


FIG. 7. (Color online) Top: the lattice thermal conductivities of infinite (Pure and Isotope) and finite-size (0.6, 0.3, 0.1, 0.06 and 0.03 μm) monolayer MoSSe as a function of temperature; Bottom: the cumulative lattice thermal conductivity of MoS₂, MoSSe and MoSe₂ monolayers divided by their total lattice thermal conductivity with respect to phonon MFP at room temperature.

To further understand phonon transports of MoS₂, MoSSe and MoSe₂ monolayers, phonon mode group velocities and lifetimes are calculated. Due to dominant contribution to total κ_L from acoustic phonon branches, we only show acoustic phonon mode group velocities and lifetimes in Figure 5 and Figure 6. From MoS₂ to MoSSe to MoSe₂ monolayer, most of group velocities become small due to softened acoustic phonon modes, which results in the decrease of the lattice thermal conductivity. The largest phonon group velocity at the Γ point of the LA/TA modes decreases from 6.60/4.11 km/s to 5.62/3.55 km/s to 5.06/3.22 km/s from MoS₂ to MoSSe to MoSe₂ monolayer. For ZA branch, the largest phonon group velocity changes from 4.18 km/s to 3.56 km/s to 3.29 km/s. Therefore, the group velocity reduction may be partial reason for the thermal conductivity reduction from MoS₂ to MoSSe to MoSe₂ monolayer. It is straightforward to find that most of phonon lifetimes of MoSSe and MoSe₂ monolayers are shorter than ones of MoS₂ monolayer, which may be due to larger acoustic and optical phonon gap. However, the phonon lifetimes be-

tween MoSSe and MoSe₂ monolayers are comparative. The lower κ_L for MoSSe/MoSe₂ than MoS₂ monolayer is due to lower group velocities and shorter lifetimes. The κ_L of MoSe₂ is lower than that of MoSSe, which is mainly due to lower group velocities.

Based on the formula proposed by Shin-ichiro Tamura⁴², phonon-isotope scattering is included, and the mass variance parameters are read from database of the natural abundance data for elements. The room temperature "isotope effect" can be measured by $P = (\kappa_{\text{pure}}/\kappa_{\text{iso}} - 1)$. The calculated value is 6.2%, which means that phonon-isotope scattering has little effects on κ_L . With increasing temperature, isotopic effect on κ_L gradually becomes weak due to enhancement of phonon-phonon scattering. In reality, finite-size sample is usually used in the device implementation. By adopting a most simple boundary scattering model, the boundary scattering rate can be obtained by v_g/L , in which v_g , L are the group velocity and boundary mean free path (MFP), respectively. The lattice thermal conductivities of infinite and finite-size (0.6, 0.3, 0.1, 0.06 and 0.03 μm) MoSSe monolayer as a function of temperature are plotted in Figure 7. It is apparent that the thermal conductivity decreases with length decreasing, which is due to enhanced boundary scattering. For the 0.6, 0.3, 0.1, 0.06 and 0.03 μm cases, the room-temperature κ_L of MoSSe monolayer is about 81.5%, 70.2%, 47.6%, 37.1% and 24.8% of one of infinite (Pure) case.

The MFP distributions over a wide range of length scales can be measured by thermal conductivity spectroscopy technique⁴³. At 300 K, the ratio between cumulative and total lattice thermal conductivity of MoS₂, MoSSe and MoSe₂ monolayers as a function of phonon MFP are shown in Figure 7, which measures how phonons with different MFP contribute to the total lattice thermal conductivity. With MFP increasing, the ratio approaches one. When the ratio reaches 99%, the corresponding MFP is 728 nm, 502 nm and 748 nm from MoS₂ to MoSSe to MoSe₂ monolayer. The critical MFP of MoSSe is smaller than that of MoS₂ or MoSe₂ monolayer, which is because MoSSe monolayer contains more element types. It is noted that critical MFP significantly depends on strain, which has been found in antimonene, silicene, germanene, and stanene^{25,27}. With κ_L reducing to half by nanostructures, the characteristic length changes from 121 nm to 111 nm to 129 nm from MoS₂ to MoSSe to MoSe₂ monolayer.

The κ_L is connected with Young's modulus by the simple relation $\kappa_L \sim \sqrt{E}$ ²⁸, and the Young's modulus can be attained from elastic constants. Due to D_{3h} symmetry, two independent elastic constants $C_{11}=C_{22}$ and C_{12} can be calculated, and the $C_{66}=(C_{11}-C_{12})/2$. Table IV lists the elastic constants C_{ij} of MoS₂, MoSSe and MoSe₂ monolayers, and they all satisfy the Born criteria of mechanical stability, namely

$$C_{11} > 0, C_{66} > 0 \quad (5)$$

The 2D Young's moduli Y^{2D} in the Cartesian [10] and

TABLE IV. For MoS₂, MoSSe and MoSe₂ monolayers, the elastic constants C_{ij} , shear modulus G^{2D} , Young's modulus Y^{2D} in Nm⁻¹, and Poisson's ratio ν dimensionless.

Name	$C_{11} = C_{22}$	C_{12}	$C_{66} = G^{2D}$	$Y_{[10]}^{2D} = Y_{[01]}^{2D}$	$\nu_{[10]} = \nu_{[01]}$
MoS ₂	131.7 (138.5 ⁸ , 130 ⁴⁵ , 130.3 ⁴⁶)	31.2 (31.7 ⁸ , 32 ⁴⁵ , 31.0 ⁴⁶)	50.3	124.3	0.24
MoSSe	119.3 (126.8 ⁸)	27.5 (27.4 ⁸)	45.9	113.0	0.23
MoSe ₂	115.6 (115.9 ⁸ , 108 ⁴⁵ , 110.1 ⁴⁶)	26.5 (24.0 ⁸ , 25 ⁴⁵ , 26.0 ⁴⁶)	44.6	109.5	0.23

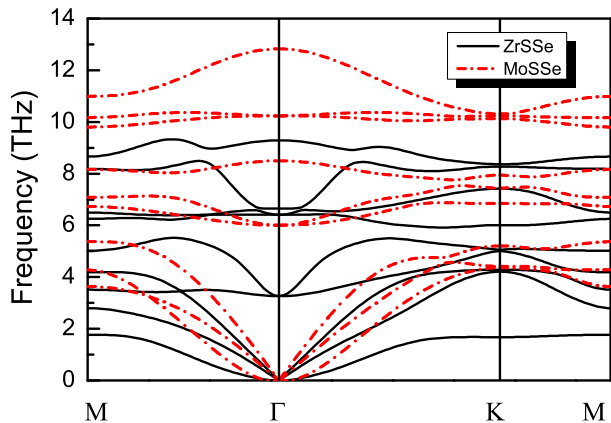


FIG. 8. Phonon dispersion curves of ZrSSe and MoSSe monolayers.

[01] directions and shear modulus G^{2D} are given⁴⁴

$$Y_{[10]}^{2D} = \frac{C_{11}C_{22} - C_{12}^2}{C_{22}}, \quad Y_{[01]}^{2D} = \frac{C_{11}C_{22} - C_{12}^2}{C_{11}} \quad (6)$$

$$G^{2D} = C_{66} \quad (7)$$

The corresponding Poisson's ratios can be expressed as:

$$\nu_{[10]}^{2D} = \frac{C_{12}}{C_{22}}, \quad \nu_{[01]}^{2D} = \frac{C_{12}}{C_{11}} \quad (8)$$

According to Table IV, the Young's modulus of MoSSe monolayer is between ones of MoS₂ and MoSe₂ monolayers, and the order of Young's modulus is identical with one of their κ_L . The calculated C_{ij} agree well with previous theoretical values^{8,45,46}, which are also listed in Table IV. It is found that the MoSSe monolayer is more flexible than MoS₂ monolayer due to smaller Young's modulus.

IV. DISCUSSIONS AND CONCLUSION

Recently, the ZrSSe monolayer is predicted by the first principle calculations¹⁰, and the calculated room-temperature sheet thermal conductance is 33.6 WK⁻¹, which is about 9.8% of one of MoSSe monolayer (342.50 WK⁻¹). The huge difference on κ_L can be understood by their phonon dispersion curves, which are shown in

Figure 8. It is clearly seen that the dispersion of acoustic branches of ZrSSe monolayer is softened with respect to MoSSe monolayer, indicating the reduction of phonon group velocity, which leads to lower κ_L for ZrSSe than MoSSe monolayer. The group velocity reduction partially explains the lower κ_L for ZrSSe than MoSSe monolayer. A frequency gap between the optical and acoustic phonon branches in MoSSe monolayer can be observed, but disappear for ZrSSe monolayer. The cross between optical and acoustic phonon branches for ZrSSe monolayer leads to much more frequent aao scattering, producing very short phonon lifetimes. The gap for MoSSe monolayer makes aao scattering ineffective, resulting in very long phonon lifetimes. The phonon lifetimes of ZrSSe are almost one order-of-magnitude smaller than that of MoSSe, which can lead to very lower κ_L for ZrSSe than MoSSe monolayer.

Strain effects on κ_L of various 2D materials have been investigated^{19,24,26,27}. For penta-SiN₂, a planar structure can be achieved from a buckled structure by tensile strain, and the κ_L jumps up by 1 order of magnitude²⁴, which is because the reflection symmetry selection rule strongly restricts anharmonic phonon scattering. For penta-SiC₂, the κ_L exhibits an unusual nonmonotonic up-and-down behavior²⁴. For MoTe₂, the κ_L shows monotonic reduction due to the reduction in phonon group velocities and phonon lifetime¹⁹. Therefore, it is very interesting to investigate the strain influence on κ_L of MoSSe monolayer.

In summary, based on phonon Boltzmann equation within the single-mode RTA, the κ_L of MoSSe monolayer is investigated together with MoS₂ and MoSe₂ monolayers. Calculated results show that the κ_L of MoSSe monolayer is very lower than that of MoS₂ monolayer, which is due to the smaller group velocities and shorter phonon lifetimes for MoSSe than MoS₂ monolayer. However, the κ_L of MoSSe monolayer is higher than that of MoSe₂ monolayer, which is mainly due to larger group velocities. It is expected that the order of Young's modulus is MoS₂ > MoSSe > MoSe₂, which is identical with that of κ_L . The isotope effect and size dependence of κ_L of MoSSe monolayer are also investigated, which is useful for designing nanostructures. This work presents comprehensive investigations on the phonon transport of Janus monolayer MoSSe, which is useful for further study in TMD Janus monolayers.

ACKNOWLEDGMENTS

This work is supported by the National Natural Science Foundation of China (Grant No.11404391). We are grateful to the Advanced Analysis and Computation Center of CUMT for the award of CPU hours to accomplish this work.

-
- ¹ K. S. Novoselov et al., *Science* **306**, 666 (2004).
² M. Chhowalla, H. S. Shin, G. Eda, L. J. Li, K. P. Loh and H. Zhang, *Nature Chemistry* **5**, 263 (2013).
³ S. L. Zhang M. Q. Xie, F. Y. Li, Z. Yan, Y. F. Li, E. J. Kan, W. Liu, Z. F. Chen, H. B. Zeng, *Angew. Chem.* **128**, 1698 (2016).
⁴ J. P. Ji, X. F. Song, J. Z. Liu et al., *Nat. Commun.* **7**, 13352 (2016).
⁵ R. X. Fei, W. B. Li, J. Li and L. Yang, *Appl. Phys. Lett.* **107**, 173104 (2015).
⁶ S. Balendhran, S. Walia, H. Nili, S. Sriram and M. Bhaskaran, *small* **11**, 640 (2015).
⁷ A. Y. Lu, H. Y. Zhu, J. Xiao et al., *Nature Nanotechnology* **12**, 744 (2017).
⁸ L. Dong, J. Lou and V. B. Shenoy, *ACS Nano* **11**, 8242 (2017).
⁹ F. P. Li, W. Wei, P. Zhao, B. B. Huang and Y. Dai, *J. Phys. Chem. Lett.* **8**, 5959 (2017).
¹⁰ S. D. Guo, arXiv:1712.09064 (2017).
¹¹ X. K. Gu and R. G. Yang, *Appl. Phys. Lett.* **105**, 131903 (2014).
¹² S. D. Guo and J. T. Liu, *Phys. Chem. Chem. Phys.* **19**, 31982 (2017).
¹³ G. H. Zheng, Y. L. Jia, S. Gao and S. H. Ke, *Phys. Rev. B* **94**, 155448 (2016).
¹⁴ S. D. Wang, W. H. Wang and G. J. Zhao, *Phys. Chem. Chem. Phys.* **18**, 31217 (2016).
¹⁵ Z. Z. Qin, G. Z. Qin, X. Zuo, Z. H. Xiong and M. Hu, *Nanoscale* **9**, 4295 (2017).
¹⁶ B. Peng, H. Zhang, H. Z. Shao, Y. C. Xu, X. C. Zhang and H. Y. Zhu, *RSC Adv.* **6**, 5767 (2016).
¹⁷ T. Zhang, Y. Y. Qi, X. R. Chen and L. C. Cai, *Phys. Chem. Chem. Phys.* **18**, 30061 (2016).
¹⁸ S. D. Guo, A. X. Zhang and H. C. Li, *Nanotechnology* **28**, 445702 (2017).
¹⁹ A. Shafiqe and Y. H. Shin, *Phys. Chem. Chem. Phys.* **19**, 32072 (2017).
²⁰ S. D. Guo, *J. Mater. Chem. C* **4**, 9366 (2016).
²¹ B. Peng, D. Q. Zhang, H. Zhang, H. Z. Shao, G. Ni, Y. Y. Zhu and H. Y. Zhu, *Nanoscale* **9**, 7397 (2017).
²² H. Y. Lv, W. J. Lu, D. F. Shao, H. Y. Lub and Y. P. Sun, *J. Mater. Chem. C* **4**, 4538 (2016).
²³ G. P. Li, G. Q. Ding and G. Y. Gao, *J. Phys.: Condens. Matter* **29**, 015001 (2017).
²⁴ H. K. Liu, G. Z. Qin, Y. Lin and M. Hu, *Nano Lett.* **16**, 3831 (2016).
²⁵ A. X. Zhang, J. T. Liu, S. D. Guo and H. C. Li, *Phys. Chem. Chem. Phys.* **19**, 14520 (2017).
²⁶ L. Lindsay, Wu Li, J. Carrete, N. Mingo, D. A. Broido and T. L. Reinecke, *Phys. Rev. B* **89**, 155426 (2014).
²⁷ Y. D. Kuang, L. Lindsay, S. Q. Shic and G. P. Zheng, *Nanoscale* **8**, 3760 (2016).
²⁸ W. Kim, *J. Mater. Chem. C* **3**, 10336 (2015).
²⁹ G. Kresse, *J. Non-Cryst. Solids* **193**, 222 (1995).
³⁰ G. Kresse and J. Furthmüller, *Comput. Mater. Sci.* **6**, 15 (1996).
³¹ G. Kresse and D. Joubert, *Phys. Rev. B* **59**, 1758 (1999).
³² J. P. Perdew, K. Burke and M. Ernzerhof, *Phys. Rev. Lett.* **77**, 3865 (1996).
³³ A. Togo, L. Chaput and I. Tanaka, *Phys. Rev. B* **91**, 094306 (2015).
³⁴ A. Togo, F. Oba, and I. Tanaka, *Phys. Rev. B* **78**, 134106 (2008).
³⁵ X. F. Wu, V. Varshney et al., *Chem. Phys. Lett.* **669**, 233 (2017).
³⁶ X. Zhang, X.-F. Qiao, W. Shi, J.-B. Wu, D.-S. Jiang and P.-H. Tan, *Chem. Soc. Rev.* **44**, 2757 (2015).
³⁷ D. J. Late, S. N. Shirodkar, U. V. Waghmare, V. P. Dravid and C. N. R. Rao, *ChemPhysChem* **15**, 1592 (2014).
³⁸ L. Lindsay, D. A. Broido and T. L. Reinecke, *Phys. Rev. Lett.* **111**, 025901 (2013).
³⁹ X. Gu and R. Yang, *Appl. Phys. Lett.* **105**, 131903 (2014).
⁴⁰ L. Lindsay, D. Broido, and T. Reinecke, *Phys. Rev. Lett.* **111**, 025901 (2013).
⁴¹ L. Lindsay, D. Broido, and T. Reinecke, *Phys. Rev. B* **87**, 165201 (2013).
⁴² S.I. Tamura, *Phys. Rev. B*, **27**, 858 (1983).
⁴³ A. J. Minnich, J. A. Johnson, A. J. Schmidt, K. Esfarjani, M. S. Dresselhaus, K. A. Nelson and G. Chen, *Phys. Rev. Lett.* **107**, 095901 (2011).
⁴⁴ R. C. Andrew, R. E. Mapasha, A. M. Ukpogon and N. Chetty, *Phys. Rev. B* **85**, 125428 (2012).
⁴⁵ K. A. N. Duerloo, M. T. Ong and E. J. Reed, *J. Phys. Chem. Lett.* **3**, 2871 (2012).
⁴⁶ M. N. Blonsky, H. L. Zhuang, A. K. Singh and R. G. Hennig, *ACS Nano* **9**, 9885 (2015).